Article

Identification of Myricetin as Ebolavirus VP35-dsRNA interaction inhibitor through a novel fluorescence-based assay

Gian Luca Daino, Aldo Frau, Cinzia Sanna, Daniela Rigano, Simona Distinto, Veronica Madau, Francesca Esposito, Elisa Fanunza, Giulia Bianco, Orazio Taglialatela-Scafati, Luca Zinzula, Elias Maccioni, Angela Corona, and Enzo Tramontano

Biochemistry, **Just Accepted Manuscript** • DOI: 10.1021/acs.biochem.8b00892 • Publication Date (Web): 09 Oct 2018

Identification of Myricetin as Ebolavirus VP35-dsRNA interaction inhibitor through a novel fluorescence-based assay

Gian Luca Daino[1], Aldo Frau[1], Cinzia Sanna[1], Daniela Rigano[2], Simona Distinto[1], Veronica Madau[1], Francesca Esposito[1], Elisa Fanunza[1], Giulia Bianco[1], Orazio Taglialatela-Scafati[2], Luca Zinzula[3], Elias Maccioni[1], Angela Corona[1] and Enzo Tramontano[1,4*]

[1]Department of Life and Environmental Sciences, University of Cagliari, Cagliari,09042, Italy.
[2]Department of Pharmacy, School of Medicine and Surgery, University of Naples Federico II, Naples, 80131, Italy.
[3]The Max-Planck Institute of Biochemistry, Department of Molecular Structural Biology, Martinsried, 82152, Germany.
[4]Istituto di Ricerca Genetica e Biomedica, Consiglio Nazionale delle Ricerche (CNR), Monserrato, 0942, Italy.

*To whom correspondence should be addressed. Tel: +39-0707654538 Fax: +39-0706754536 Email: tramon@unica.it

ABSTRACT

Ebola virus (EBOV) is a filovirus that causes a severe and rapidly progressing hemorrhagic syndrome whose recent epidemic enlightened the urgent need of novel therapeutic agents, since no drug is currently approved. A key contribution to the high lethality observed during EBOV outbreaks comes from viral evasion of the host antiviral innate immune response in which the viral protein VP35 plays a crucial role, blocking the interferon type I production, firstly by masking the viral dsRNA and preventing its detection by the pattern recognition receptor RIG-I. Aiming to identify inhibitors of VP35 interaction with the viral dsRNA, counteracting the VP35 viral innate immune evasion, we established a new methodology for high-yield recombinant VP35 (rVP35) expression and purification, and a novel and robust fluorescence-based rVP35-RNA interaction assay (Z'-factor of 0.69). Taking advantage of such newly-established methods, we screened a small library of Sardinian natural extracts finding *Limonium morisianum* as the most potent inhibitor extract. A bio-guided fractionation led to the identification of myricetin as the component able to inhibit rVP35-dsRNA interaction with an IC_{50} value of 2.7 μM. Molecular docking studies showed that myricetin interacts with the highly conserved region of the VP35 RNA binding domain, laying the basis for further structural optimization of potent VP35-dsRNA inhibitors.

INTRODUCTION

The recent *Zaire ebolavirus* (EBOV) epidemic occurred in West Africa in 2013-2016 has awakened the international scientific and political communities to the need of finding a cure for Ebola virus disease (EVD), a severe, frequently fatal hemorrhagic syndrome in humans and non-human primates[1]. EBOV belongs to a viral genus that includes 6 species of filamentous, enveloped, non-segmented negative single-strand RNA viruses, among which it is the one causing most of the epidemics reported to date[2,3]. The average case fatality rate was reported to be around 40% for the recent EBOV West Africa outbreak [4], while it varied from 25% to 90% in the several outbreaks occurring over the past decades [5]. Given its high virulence and the consequent ability to induce panic, EBOV is classified by the Centers of Diseases Control and Prevention (CDC) as Category A biowarfare agent [6]. Even if the experimental administration of few drugs has been attempted to treat patients during the last EVD epidemics, therapy is still mainly based on early-aggressive supportive care with rehydration, and no approved vaccine [7] or drug [8] is currently available.

Among the different pathogenic mechanisms involved in EVD, a key contribution to high lethality comes from EBOV suppression of the host antiviral innate immune response that involves two viral proteins, VP24 and VP35 [9–11]. In fact, it is known that, during infection, viral components are detected by host pattern recognition receptors (PRRs) such as Toll-like receptors (TLRs) and retinoic acid inducible gene-1 (RIG-I) like receptors (RLRs), which trigger antiviral innate immune response through the production of type I interferon (IFN-α/β). Particularly, the viral double-stranded RNA (dsRNA) produced in the cytoplasm during EBOV replication is recognized by RLRs [12]. EBOV is able to block IFN production in response to viral dsRNA detection through its VP35 protein, a multifunctional protein that is also a structural component of the viral nucleocapsid and an indispensable cofactor for the viral polymerase during replication and transcription [13]. VP35 inhibits the induction of IFN-α/β expression in a dose dependent manner [14] through multiple mechanisms: i) interacting with dsRNA to prevent RIG-I and melanoma differentiation-associated gene 5 (MDA-5) activation [15,16]; ii) binding to Protein ACTivator of the interferon-induced protein kinase (PACT) to inhibit its interaction with RIG-I and PACT-induced RIG-I ATPase activity [17]; iii) binding to TANK-binding kinase 1 (TBK-1) and IκB kinase epsilon (IKK_ε), suppressing their kinase activities [18], to block the virus-induced phosphorylation and activation of IFN regulatory factor 3 (IRF-3) [19]; iv) associating non-covalently with polyubiquitin chains to inhibit the TRIM6-mediated IFN-I induction [20]; v) repressing the stress granule assembly [21]. Therefore, given its multifunctional nature and the multiple roles in EBOV infection and pathogenesis, VP35 is a major target for drug development against EBOV [22].

EBOV VP35 is a 340 amino acid protein that contains an N-terminal domain [23] and a C-terminal RNA-binding domain (RBD) [24,25] whose structure has been solved in complex with short dsRNA molecules and small molecule inhibitors, that inhibit VP35-viral nucleoprotein (NP) interaction [25–28]. VP35 binds dsRNA

as an asymmetric RBD dimer that wrap around dsRNA termini. Within each dimer, one monomer (the so-called end-capping RBD) interacts with the dsRNA terminal bases, whereas the other one (referred to as the backbone-binding RBD) interacts with the nucleic acid phosphate groups (26). RBD is also termed interferon inhibitory domain (IID), as it is sufficient to exert VP35 IFN inhibition properties, even if as a single domain it is not able to suppress the type I IFN activation at the same level of the full length protein [15,23,29,30]. Between the RBD and N-terminal domain there is a coiled-coil (CC) domain that mediates VP35 homo-oligomerization [31], essential for VP35 interaction with the viral polymerase L and for maximal suppression of IFN production [23,32]. The N-terminal domain has at its end a 28 amino acid residues-long peptide which releases the viral RNA by displacing the NP protomers of the nucleocapsid and exerts a chaperone function guiding free NPs on the de novo synthesized viral genome [33–35].

Although a rapid accumulation of genetic variations in the EBOV genome has been observed in the last epidemic of West Africa [36], the VP35 RBD contains a highly conserved α-β basic patch whose residues (Ala-238, Gln-241, Leu-242, Val-245, Ile-246, Leu-249, Ile-278, Ile-280, and Phe-287 that form a α-helical subdomain and Pro-293, Ala-306, Cys-307, Pro-315, Pro-318, Ile-320, Asp-321, Gly-323, Trp-324, Val-325, Leu-338, and Ile-340 that from a β-sheet subdomain) are important for dsRNA binding in a sequence independent manner [25,37]. Mutations in the VP35 RBD that suppress the VP35 binding ability to dsRNA have been shown to lead to the loss of EBOV virulence in animal models [38,39], strongly suggesting that VP35 ability to bind viral dsRNA is critical to prevent viral detection by cytoplasmic PRRs and it is therefore a key target in EBOV drug discovery [22].

Despite its pivotal role in EBOV replication and pathogenesis, the molecular characterization of VP35 has been hampered for a long time by the difficulties to produce a recombinant full length VP35 (rVP35) in bacteria, due to the fact that viral dsRNA binding proteins can exert a toxic effect on *E. coli* cells or show anomalous dsRNA binding due to the binding of bacterial RNA [40]. After the first production of limited amounts of a heavily truncated version (amino acids 171–339) [15], the full-length rVP35 has been expressed in *E. coli*, purified as soluble His-tagged protein [41] and used to validate an *in vitro* pull-down assay based on a ^{3}H-labeled 500 bp dsRNA (^{3}H-dsRNA) to screen small molecules targeting VP35-dsRNA interaction [42]. Even though limited by low protein yield and not suited for high-throughput scale-up, the published method provided a first tool to target full-length VP35-dsRNA interaction, while all the other studies on this topic used only the RBD [15,26,27,37,43–45]. Of note, investigations on the VP35 RBD led to the identification of small molecules and RNA aptamers that disrupts the interaction between VP35 and the viral NP, targeting its polymerase co-factor function [28,46]. Hence, no molecule able to inhibit VP35-dsRNA interaction has been identified yet.

The use of plants and plant extracts has been the first therapeutic strategy for humans [47], but it suffered a progressive decline over the past decades in favor of synthetic drugs [48]. In particular, the Mediterranean area offers a great variety of endemic plants and the Sardinia island, where geographical isolation determined an even greater plant biodiversity with significant variations in genetic and molecular

characteristics as compared to plants grown in other regions, offers good opportunities for the identification of novel metabolites endowed of biological activities [49–58].

In this study, we firstly implemented the full-length rVP35 purification protocol to obtain high yield protein and established a novel biochemical assay to measure the VP35-dsRNA binding based on the use of a fluorescent dsRNA oligomer ligand, instead of the radioactive substrate, and 96-wells nickel-coated plates instead of the paramagnetic beads previously used. We calculated the equilibrium dissociation constant (K_d) and maximum binding capacity (B_{max}) for the VP35-dsRNA binding, and validated the assay determining its Z'-factor. Next, we screened a small library of Sardinian plant extracts showing that the *Limonium morisianum* Arrigoni methanol extract inhibits the VP35-dsRNA binding. Bio-guided purification of the extract showed that the flavonol myricetin is the component responsible for VP35-dsRNA binding inhibition. Blind docking studies were carried out to predict the myricetin binding mode showing that it binds to the VP35 dsRNA binding pocket, thus offering the possibility of designing potent VP35 inhibitors.

MATERIAL AND METHODS

Plasmid construction, cloning and protein expression

Cloning of the EBOV VP35 gene in pET45b(+) vector (Novagen) and production of pET45b-EBOV-VP35 plasmid for the expression of recombinant N-terminal His6-tag-VP35 protein was performed as previously described [41]. BL21AI *E. coli*competent for transformation (Invitrogen) were prepared and transformed with pET45b-EBOV-VP35 plasmid. Transformants were selected on Luria-Bertani (LB) agar plates containing 150 µg/ml of ampicillin. A transformed bacterial colony was inoculated in 50 ml of LB medium containing 150 µg/ml ampicillin and left to grow overnight (ON) at 200 rpm at 37 °C. Bacterial culture was transferred in 4 liters LB medium containing 150 µg/ml ampicillin and 0.1 % (w/v) glucose and incubated at 37 °C with shaking (200 rpm) until 0.6 OD_{600}. Protein expression was induced adding 0.4 % (w/v) L-arabinose and 0.65 mM Isopropil-β-D-1-tiogalattopiranoside, and culture was incubated ON at 200 rpm at 18 °C. After incubation, the cell culture was centrifuged at 4500xg at 4 °C for 20 min and bacterial pellets were collected and frozen at -80 °C.

Protein purification: denaturation and refolding

The bacterial pellet was re-suspended in 5:1 ml of lysis buffer (100 mM sodium phosphate pH 8.0, 500 mM NaCl, 1 mM 2-mercaptoethanol, 10 % glycerol, 20 mM imidazole, 6 M urea). The suspension was incubated on ice for 15 min and subsequently sonicated on ice. The cell lysate was centrifuged at 32,000xg at 4 °C for 45 min. The purification was performed in a BioLogic LP Chromatographic System (Biorad). Supernatant was loaded (0.5 ml/min) to an Econo Column (Biorad) packed with 3 ml of Ni-Sepharose High Performance (GE Healthcare), pre-equilibrated in binding buffer (100 mM sodium phosphate pH 8.0, 300 mM NaCl, 1 mM 2-mercaptoethanol, 10 % glycerol, 20 mM imidazole, 6 M urea). Urea content was gradually removed from the column by a decreasing gradient of concentration from 6 up to 0 M with a flow rate of 0.5 ml/min for around 130 column volumes (800 minutes). The column was washed for 40 column volumes with three Washing buffers (50 mM sodium phosphate pH 8.0, 300 mM

NaCl, 1 mM 2-mercaptoethanol, 10% glycerol) with increasing concentrations of imidazole (70 mM - 150 mM - 250 mM). Refolded recombinant protein was eluted using 90 ml of the same buffer having 1 M imidazole and fractions collected. Significant eluted fractions, selected on IMAC chromatogram, were analyzed in a 12% SDS–PAGE. Fractions containing pure rVP35 protein were gathered and dialyzed against Dialysis buffer (50 mM sodium phosphate pH 8.0, 800 mM NaCl, 1 mM 2-mercaptoethanol, 10% glycerol). Afterwards, protein concentration was determined by Bradford assay with the Protein Quantification Kit-Rapid (Fluka – Sigma Aldrich).

Immunoblot analysis

VP35 recombinant protein was run in 12% sodium dodecyl sulfate-polyacrylamide gel (SDS-PAGE) (Thermo-Scientific) and then transferred to a polyvinylidene difluoride (PVDF) (Thermo-Scientific) membrane by standard methods. Membranes were blocked with 5% nonfat dry milk in TBS-T (20 mM Tris-HCl, 137 mM NaCl, 0.05% Tween 20, pH 7.4) and probed with 1μg/mL of mouse 6x-His Tag monoclonal antibody (Invitrogen) and HRP-linked anti-mouse IgG secondary antibody (1:10000) (Life Technologies). Detection was performed using Pierce ECL Western Blotting Substrate and Chemidoc MP Imaging System (Biorad).

Preparation of dsRNA substrates

500 bp dsRNA was produced by *in vitro* transcription (IVT) using the T7 MEGAscript RNAi kit (Ambion) from the linearized DNA provided with the kit as template, according to manufacturer's instructions. IVT oligomers were purified from transcription reaction with Quick Spin G25 columns (Roche), following manufacturer instructions, and quantified by spectrophotometry. Similarly, a 500 bp radiolabeled dsRNA was obtained by supplementing the *in vitro* transcription reaction with 0.15 μCi of ^{3}HGTP (35.5 Ci/mmol). A fluorescence-labeled dsRNA oligomer of 30 bp in length and an unlabeled 30 bp oligomer were prepared by annealing from three different ssRNA purchased from Metabion International AG (Germany). Sequences purchased were: a) 5'-ppp-cccuuuccuccuuccuuuuguuccucuccc-3', b) 5'-gggagaggaacaaaaggaaggaggaaaggg-3', c) 5'-Fluorescein-gggagaggaacaaaaggaaggaggaaaggg-3'. Annealing has been conducted in order to have in each dsRNA molecule one 5'-triphosphate end. The integrity of DNA templates, IVT dsRNAs and synthetic dsRNA molecules were assessed by agarose-gel electrophoresis.

Magnetic pull-down assay

First phase of the magnetic pull-down assay was the conjugation between 2 μg of rVP35 and 2 mg of paramagnetic Talon Dynabeads (Invitrogen) in a volume of 700 μl of binding/washing buffer (50 mM Sodium Phosphate pH 7.5, 150 mM NaCl, 0.03 % Tween-20) for 30 minutes at 4 °C under gentle rotating agitation (20 rpm). Applying a magnetic field, supernatant with unconjugated rVP35 was removed and beads washed twice with binding/washing buffer. Pellets with conjugated rVP35 were re-suspended in a reaction mixture having 50 mM Sodium Phosphate pH 7.5, 100 mM NaCl, 20 mM $MgCl_2$, 0.03% Tween-

20, transferred in a 96-multiwell plate in conjunction with labeled, and eventually not labeled, dsRNA (depending on the type of experiment to be carried out) up to a final volume of 100 µl and incubated for 60 min at 37 °C (200 rpm). After incubation, supernatant with unbound dsRNA was removed under the application of magnetic field, followed by two rounds of washing with 200 µl of washing buffer to remove it entirely. After 10 min incubation at room temperature with 200 µl of elution buffer (50 mM Sodium Phosphate pH 7.5, 300 mM NaCl, 1 M imidazole, 0.03% Tween-20), supernatant containing the complex rVP35-dsRNA was recovered and either measured at a beta-counter to determine its radioactive signal, as previously described [42] or transferred into a black 96-multiwells plate to determine the fluorescence signal with Multilabel counter plate reader Victor 3 (Perkin Elmer model 1420-051) equipped with filters for 490/528 nm (excitation/emission wavelength).

Determination of the kinetic parameters

K_d and B_{max} values for the binding between rVP35 and 30 bp dsRNA were determined using two approaches. The first method consisted in performing two parallel saturation experiments using increasing concentrations 30 bp dsRNA labeled on its 5'-end with a fluorescein ligand and the second one with same concentrations of fluorescence-labeled 30 bp dsRNA in the presence of a fixed concentration of unlabeled 30 bp dsRNA. Both experiments were performed with the magnetic pull-down and the nickel-coated plate method.

In the magnetic pull-down assay the concentration of labeled dsRNA ranged from 1.5 to 200 nM, while the one of unlabeled dsRNA was 2 µM. In the Nickel-coated plates assay, the concentrations of labeled dsRNA ranged from 0.125 to 32 nM, while the one of unlabeled dsRNA was 200 nM. Values obtained were analyzed both by Scatchard-plot analysis and by a non-linear regression, in order to calculate K_d and B_{max} values [59].

The second method consisted in a homologous competition assay where a fixed concentration of labeled 30bp dsRNA (7.5 nM) competed for the binding to rVP35 with increasing concentrations of unlabeled 30bp dsRNA (ranging from 0.15 nM to 500 nM).

For the calculation of the kinetic parameters through non-linear regression model, it was used the GraphPad Prism 6. K_d and B_{max} values were calculated using the simplification of the Cheng and Prussof equation presented by De Blasi et al. [60] starting from the values of IC_{50} and B_0, following the equations $K_d = IC_{50} – L$ and $B_{max} = B_0\ IC_{50} / L$ (where B_0 is the difference between the concentration of the higher plateau minus that of the lower plateau and L is the concentration of labeled 30bp dsRNA) [59,60].

Plant extracts preparation and chromatographic separation

The aerial parts of *Clinopodium nepeta* (L.) Kuntze (voucher specimen Herbarium CAG 1082), *Mentha pulegium* L. (voucher specimen Herbarium CAG 1072), *Solanum linnaeanum* Hepper & P.-M.L. Jaeger (voucher specimen Herbarium CAG 989) and *Limonium morisianum* Arrigoni (voucher specimen Herbarium CAG 909/G) were dried in a ventilated stove and then extracted with MeOH (3 × 1 L, 8 h each), filtered and evaporated to obtain crude extracts tested for inhibition of EBOV-VP35 binding to

dsRNA (Table 1). In order to evaluate their effects on the rVP35 binding to dsRNA, dry plant extracts were resuspended in DMSO at concentration of 2.5 mg/ml at consecutively diluted in water.

The crude methanolic extract of *L. morisianum* (22 g) was dissolved in water and then successively partitioned against EtOAc and *n*-butanol, to afford EtOAc, *n*-BuOH, and H_2O phases. The EtOAc phase was dissolved in methanol and then successively defatted through partitioning against *n*-hexane. The residual methanol phase (3 g) was subjected to Medium Pressure Column Chromatography (MPLC) over a silica gel column (230–400 mesh) eluting with a solvent gradient of increasing polarity from *n*-hexane to EtOAc, EtOAc/MeOH (1:1), and finally MeOH. A total of nine fractions were obtained. Fraction 8 (90 mg) was purified by reverse-phase HPLC (H_2O/ACN 80:20, 0,15% TFA, flow rate 1.0 mL/min) on a Knauer apparatus equipped with a refractive index detector to afford pure myricetin (1, 20.0 mg). Fraction 9 (300 mg) was purified under the same conditions to afford (-)-epigallocatechin 3-O-gallate (EGCG) (2, 36.0 mg). The compounds were identified on the basis of their MS (LTQ OrbitrapXL Thermo Scientific) and NMR (Varian INOVA 500 MHz spectrometer) data [47].

Nickel-coated plates assay

In a Pierce® Nickel Coated Plate (Thermo Fisher) the amount of rVP35 needed to saturate Nickel-coated plate well binding capacity (700 ng) was added in each well in a volume of 200 µl of coating buffer (final concentration 50 mM Sodium Phosphate pH 7.5, 150 mM NaCl) and incubated for 30 min at 4 °C under rotating agitation (120 rpm), then washed twice with 200 µl of washing buffer (50 mM Sodium Phosphate pH 7.5, NaCl 150 mM, 0.03 % Tween-20). After removing supernatant, a volume of 100 µl was added with 7.5 nM of 30 bp 5'-fluorescein-dsRNA in a reaction mixture having 50 mM Sodium Phosphate pH 7.5, 100 mM NaCl, 20 mM $MgCl_2$, 0.03 % Tween-20. When extracts and compounds were tested, different serial dilutions of extracts or compounds were added together with the 30 bp 5'-fluorescein-dsRNA and a short dsRNA oligomer was used as positive control for the inhibition. The plate was incubated for 60 min at 37 °C (200 rpm). After the incubation, unbound dsRNA was removed by two washing with 200 µl of a reaction mixture and then, adding 200 µl of the same buffer, fluorescence signals of samples were read with the above-mentioned plate reader (Victor 3 -Perkin-Elmer). IC_{50} values were determined by GraphPad Prism 6.

The Z'-factor value was calculated from the following equation developed by Zhang et al [61]

$$Z' = 1 - 3 * \frac{(SD\ signal\ + SD\ background)}{Msignal\ - Mbackground}$$

where SD signal is the standard deviation of the positive control signal, SD background is the standard deviation of the negative control, M signal is the mean of the positive control, and M background is the mean of the negative control. All experiments were repeated at least three times. Quantitative data were expressed as the mean ± SD.

Docking of Myricetin on EBOV VP35

Ligand preparation. Myricetin was docked in the global minimum energy conformation as determined by molecular mechanics conformational analysis performed with Macromodel software [62]. The protocol consisted in 1000 steps with an energy window for saving structure of 10 kJ/mol. The algorithm used was the Monte Carlo method with MMFFs (Merck molecular force fields) [63] water implicit solvation model and the Polak-Ribier Coniugate Gradient (PRCG) method, converging on gradient with a threshold of 0.01 kJ(mol•Å)-1 [64].

Protein preparation. The protein structure was obtained from the PDB web site with pdb code 3L25[37]. The protein was prepared by using the protein preparation wizard [65].

Blind Docking experiments. Docking were conducted by applying Glide [66] XP, AutoDock [67], QMPL [68] (XP) and AutoDockVina [69] docking programs. All settings were left as default. We only decided to choose a higher number of energy evaluations to ensure a sufficient sampling of the conformational space of the ligands (5M) and 100 runs for Autodock and 32 as exhaustiveness for AutodockVina. For all programs the whole enzyme was considered in the docking experiments in order to identify the preferred binding site. Depictions were taken by means of Pymol [70] and Maestro GUI [65].

RESULTS AND DISCUSSION

rVP35 purified under denaturing conditions still binds dsRNA

The mentioned biochemical *in vitro* assay for the screening of antiviral agents targeted to VP35-dsRNA interaction [42] and the related methods of purification of full-length rVP35 [41] were affected by two limiting factors: firstly, the amount of available rVP35 coming from IMAC was very limited, since after the expression of rVP35 in *E. coli* most of the protein was retrieved in the inclusion bodies, resulting in time-consuming efforts to produce the needed amount of protein. Secondly, the binding experiments were performed using a ^{3}H-GTP-labeled dsRNA, a radioactive molecule that makes the assay expensive and hazardous. To improve the yield of purification we developed a protocol based on the recovery of rVP35 from inclusion bodies by denaturation in urea. It is known that the conversion of aggregated proteins into soluble and biologically active proteins could be done by different methods, however, the on-column refolding during the chromatography gives better quality proteins and higher yield [71], therefore, rVP35 expressed in *E. coli* was denatured with high urea concentrations and then refolded on-column. After elution, fractions were collected and analyzed by SDS-PAGE that showed a main band corresponding to a molecular weight of ~40 kDa and one fainter around 80 kDa (Figure.1A).

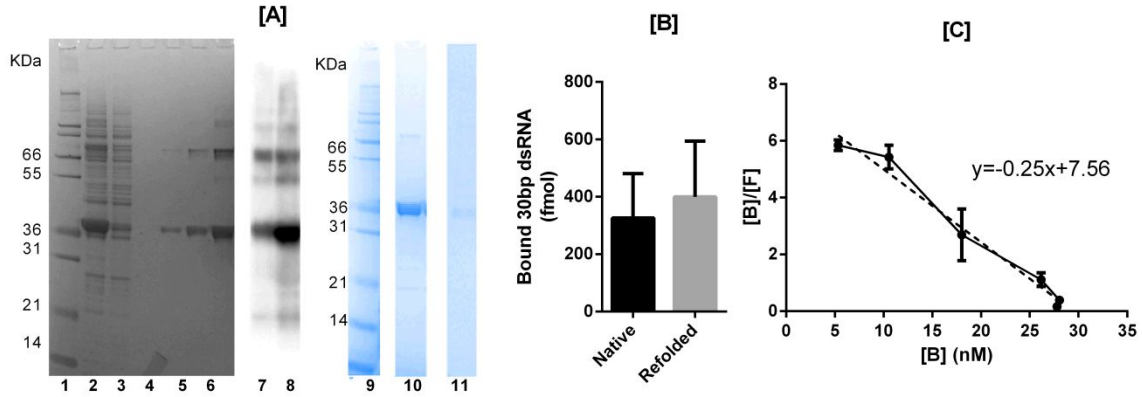

Figure. 1. Comparison between native and refolded rVP35 [A] Coomassie Blue-stained polyacrylamide gels of purification and western blot of EBOV rVP35. Lanes 1-6, denaturing conditions. 1, molecular weight marker; lane 2, crude extract cell lysate; lane 3, flow through; lane 4, washing fraction; lanes 5-6, elution fractions; lanes 7-8, western blot caption of fractions in lanes 5-6;
lane 9, molecular weight marker; lane 10, purification under denaturing conditions of EBOV rVP35, fraction correspondent to elution peak; lane 11, purification under non-denaturing conditions of EBOV rVP35, fraction correspondent to elution peak. [B] Comparison between the binding activity of EBOV rVP35 purified with native or denaturating and refolding conditions, by magnetic pull down assay. [C] Scatchard-plot analysis. Values of bound [B] and free [F] obtained with the experiment of saturation analysis were used in the Scatchard-plot analysis, obtaining that K_d = 3.9 ± 0.3 nM and B_{max} = 29.5 ± 3.7 nM.

The main band was expected at ~40 kDa, since the presence of an additional 10 amino acid-tag in rVP35 sequence brings the theoretical molecular weight to be near to 38.6 kDa. The second faint band could be interpreted as a residual dimeric form of rVP35, as previously reported for the protein purified without denaturation and subsequent refolding [41], suggesting that homo-dimerization is strong enough to resist SDS-PAGE denaturation, as it has been observed for other proteins [72]. In fact, the presence of SDS in the polyacrylamide gel should have had disrupted subunit hydrophobic interactions, their persistence even in a small percentage confirms that this binding is very stable, as recently reported [73]. In order to confirm that all bands observed in SDS-PAGE were indeed rVP35, a Western blot analysis was performed using anti-His6-tag monoclonal primary antibody, confirming that the bands were indeed EBOV rVP35 (Fig 1.A, lines 7-8). Of note, as compared to the previous methodology [41], the rVP35 yield was increased by 13-15 folds, rising from about 150 µg/l of bacterial broth, obtained under non-denaturing conditions, to approximately 2-2.5 mg/l obtained under denaturing conditions (figure 1.A lines 10-11). Consequently, it was required to verify whether the refolded high-yield purified EBOV rVP35 still had the ability of binding dsRNA. Hence, we performed the previously described magnetic pull-down assay [42], using a IVT 500 bp ^{3}HGTP-dsRNA as substrate and the rVP35 proteins obtained under both denaturing and non-denaturing conditions. Results clearly showed that both proteins were able to bind the same amount of dsRNA (figure. 1.B), demonstrating that the refolded rVP35 still retains the ability to bind dsRNA. It is worth noting that, in addition, the denaturation of rVP35 offers the further advantage of

ensuring that the protein is purified without the presence of any bacterial RNA linked to it, that might interfere in the type of assay subsequently used.

Validation of fluorescence-labeled dsRNA as substrate for rVP35-RNA binding assay

Once verified that EBOV rVP35 purified under denaturing conditions was indeed able to bind dsRNA, we wanted to establish a fluorescence-based method to be used to screen new compounds against the VP35-RNA interaction. Therefore, we designed a new fluorescence-labeled oligo RNA to be used as a substrate in order to determine the binding parameters and hence determined the values of K_d and B_{max} with different methodologies. We used the data from saturation binding assays to calculate the kinetics parameters both with non-linear regression and Scatchard-plot analysis, while the data coming from competitive binding experiments have been analyzed only by non-linear regression.

We performed a magnetic pull-down assay using a fluorescence-labeled substrate to measure the VP35–dsRNA binding and characterize this interaction. To this aim, we designed a 30 bp long dsRNA with a triphosphate in a 5' end and a fluorescein molecule in the other 5' end. The length has been chosen considering the ability of EBOV VP35 to bind dsRNA > 8 bp [15,25,27,37,42,43,74]. In order to verify whether the refolded rVP35 could really be comparable to the native rVP35, the biochemical parameters of the refolded rVP35 were determined by a series of saturation experiments. Since it was not possible to measure directly the specific binding due to the rate of non-specific binding events included in the measured signal, in order to discriminate between specific and non-specific binding, we performed two parallel saturation experiments, the first one with fluorescent dsRNA only and the second one with the same fluorescent dsRNA in the presence of high concentration non-labeled dsRNA. The excess of non-labeled RNA led to a shift of fluorescent dsRNA from the specific binding sites, so that we measured the signal coming from non-specific binding. The rVP35 dsRNA specific binding was calculated indirectly as the difference between total dsRNA binding minus non-specific dsRNA binding as described [75]. Results showed that the trend of points for nonspecific binding related to the ligand concentration is linear, as usually expected, and its value is negligible with respect to the total binding, particularly at low concentrations of fluorescent dsRNA (data not shown). A Scatchard-plot analysis was performed on the results (Figure. 1.C). The K_d and B_{max} values obtained were 3.9 ± 0.3 nM and 29.5 ± 3.7 nM, respectively, showing that the K_d value obtained for the re-folded rVP35 to dsRNA was comparable to the K_d value (3.2 nM) previously reported for the native rVP35 measured with a longer (50 bp) radioactive-labeled dsRNA substrate [42], further demonstrating that the refolded rVP35 protein has the same biochemical properties of the native rVP35.

Establishment of 96-well nickel-coated plates assays to measure rVP35-dsRNA interaction.

Since it was needed to establish a robust 96-well assay for rVP35 binding to fluorescent dsRNA, an assay with the same rVP35 protein and the same fluorescence-labeled 30 bp dsRNA was performed using Nickel-coated 96-well plates able to bind the his-tagged rVP35. At first, we determined the amount

of rVP35 needed to saturate the Nickel-coated plate well binding capacity. Increasing amounts of protein were used (from 100 ng to 900 ng, steps of 100 ng) with an excess of 5'-labeled-dsRNA (250 nM). The signal plateau was reached at 700 ng (Figure. 2.A).

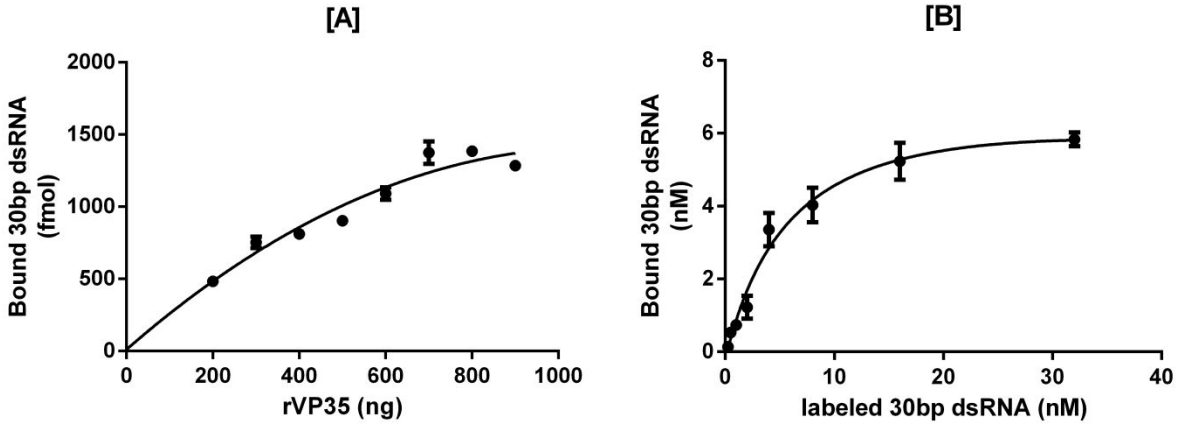

Figure. 2 Nickel-coated well/binding determination [A] Saturation analysis of well-specific binding of rVP35 to Nickel-coated plates [B] Saturation analysis of well-specific binding of dsRNA to rVP35 in Nickel-coated plate.

Of note, this amount of protein corresponds to 18 pmol of rVP35, exactly double of the value indicated for the binding capacity by the manufacturer [76], strongly pointing to the homo-dimeric nature of the rVP35 binding to the his-tagged wells. This protein amount was used to determine the optimum of dsRNA needed in the assay. A saturation curve was performed (Figure. 2.B) obtaining a K_d value of 6.6 ± 2.2 nM and the dsRNA concentration of 7.5 nM was chosen for as optimal for further experiments. Subsequently, we performed a saturation analysis with the Nickel-coated plate assay, indirectly calculating also the specific binding by non-linear regression as described above (Figure. 3.A), and obtaining a K_d value of 4.6 ± 0.5 nM and a B_{max} value of 9.0± 0.4 nM (while the K_d and B_{max} values obtained with the Scatchard-plot analysis were, respectively, 1.6 ± 0.2 nM and 8.0 ± 1.5 nM).

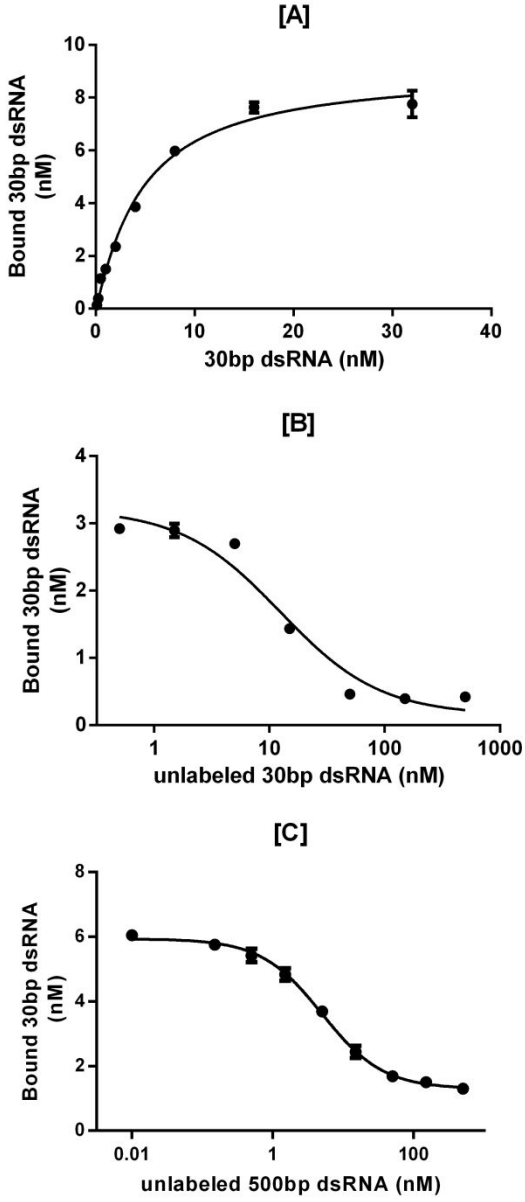

Figure. 3 Refolded rVP35 binding to dsRNAs [A] Saturation analysis of dsRNA specific binding performed with Nickel-coated plates assay. K_d value obtained through a non-linear regression was 4.6 ± 0.5 nM and B_{max} was 9.0 ± 0.4 nM. [B] Homologous competition performed with Nickel-coated plates assay. Increasing concentrations of unlabeled 30bp dsRNA from 0.5 nM to 500 nM compete with a fixed concentration of fluorescent 30bp dsRNA. [C] Heterologous competition performed with Nickel-coated plates assay. Increasing concentrations of unlabeled 500 bp dsRNA from 0.15 up to 500 nM compete with a fixed concentration of fluorescent 30 bp dsRNA.

We then performed a homologous competition assay using fixed concentration of labeled 30 bp dsRNA (7.5 nM) competed by increasing concentrations of unlabeled 30bp dsRNA (from 0.5 nM to 500 nM) (Fig.

3.B). Using the simplification of the Cheng and Prussof equation presented by De Blasi et al. [60], we then again calculated the refolded EBOV rVP35 kinetics parameters values K_d (4.95 ± 0.4 nM) and B_{max} (4.5 nM), that were comparable to the ones previously obtained. Overall the K_d data obtained were in agreement with the ones obtained in the magnetic pull-down assay showing that the Nickel-coated plate assay was reliable: K_d value obtained with homologous competition binding experiments in Nickel-coated plate assay (4.9 nM) was very close to the K_d value obtained in saturation analysis by the non-linear regression (4.6 nM) and with the one obtained in the pull-down using the Scatchard-plot analysis (3.9 nM). Additionally, we observed a difference in the B_{max} values obtained using the two different assays (29.5 nM in the pull-down and 9.0 nM in the Ni-coated plate, respectively) that were however expected, since B_{max} indicates the total number of binding sites that is obviously different in the pull-down and in the Nickel-coated plate assay. Analysis of binding between rVP35 and dsRNA reported in previous publications also gave analogous K_d values. Zinzula et al., working with full-length rVP35, obtained values of K_d, 2.8 ± 0.1 nM, 2.4 ± 0.3 nM and 3.2 ± 0.5 nM, respectively, for 500, 150, 50 bp IVT dsRNA, while using a 8 bp 5'-phosphate dsRNA the K_d value was 64 ± 9 nM [42]. Other groups, obtained for the VP35 IID alone a K_d value of 30 nM for the binding to a IVT 8 bp dsRNA containing 5′ -ppp by isothermal titration calorimetry experiments [37].

Moreover, since competitive binding experiments are used to determine whether a drug binds to the receptor [77], we used a heterologous binding experiment to confirm the validity of the assays. Since it has been previously shown that the rVP35 binding to dsRNA is dependent on the presence of 5'-ppp but does not change significantly increasing the dsRNA length [26,42], we used an unlabeled 500 bp dsRNA (ranging from 0.15 nM up to 500 nM) as competitor in a heterologous competition assay (Figure. 3.C). Results show that the 500 bp dsRNA was able to compete with the labeled 30 bp dsRNA for the binding to rVP35 with an IC_{50} value of 5.0 ± 0.4 nM. Interestingly, in all competitive binding experiments, the downhill from the maximum to the minimum plateau happened in two logarithmic unit of concentration (Figure. 3.B and 3.C) meaning that labeled and unlabeled ligands compete for a single binding site [77]. Finally, for a further validation of the assay, the Z'-factor was calculated, obtaining a value equal to 0.69, which is indicative of a robust assay [61]. Overall, such an assay will be useful to identify VP35 inhibitors and to biochemically investigate the impact of VP35 amino acid mutations that were hypothesized to have an impact on dsRNA binding and oligomerization[23,27,43,78].

Screening natural molecules on EBOV rVP35-dsRNA binding assay.

To fight highly pathogenic viruses, antiviral drugs of natural origin are an attractive source to exploit given that a number of small molecules of plant origin are already known for their antiviral effects [58,79–81], even if no antiviral drug based on these natural compounds has been approved so far. Sardinian plants are a good source of characteristic secondary metabolites with potential biological activities considering their endemic nature. Thus, we have tested some extracts from Sardinian plants to identify new molecules that may be used as antiviral agents to subvert EBOV VP35 effects or as lead compounds for a further drug

development. Herbal extracts of *Clinopodium nepeta*, *Mentha pulegium*, *Solanum linnaeanum and Limonium morisianum* have been tested in the fluorescence-based rVP35-dsRNA interaction assay (Table 1).

Table 1. Inhibition of EBOV-VP35 binding to dsRNA by Sardinian plants extracts.

Plant extract	[a]IC_{50} (µg/ml)
Calamintha nepeta	> 100 (85%)[b]
Mentha pulegium	> 100 (61%)
Solanum sodomaeum	> 100 (87%)
Limonium morisianum Arrigoni	19.2 ± 6.7
dsRNA 30 bp	12.5 ± 4.3[c]

[a]Extract concentration required to inhibit rVP35 binding to dsRNA by 50%. Data show mean ± standard deviation of at least three independent experiments.
[b]Percentage of rVP35 control binding value to dsRNA in the presence of 100 µg/ml extract concentration.
[c]Concentration expressed in nM.

Out of the four plant extracts screened, only *L. morisianum* proved to inhibit the VP35-dsRNA binding at the concentration of 19 µg/ml (Table 1). Of note, the therapeutic use of plants of the *Limonium* genus has been reported [82–85] and *L. morisianum* is an endemic Sardinian species with a characteristic composition and some potential anti HIV-1 activity [86]. Thus, the active extract was fractioned with a solvent gradient of increasing polarity obtaining several fractions, which were tested for their ability to inhibit the VP35-dsRNA binding. Results showed that fraction 8 was the one with the lowest IC_{50} value (2.1 ± 0.8, Table 2), followed by fraction 9 (4.9 ± 3.8 µg/ml, Table 2)

Table 2. Inhibition of EBOV-VP35 binding to dsRNA by *Limonium morisianum* Arrigoni fractions and main component.

Limonium morisianum Arrigoni	[a]IC_{50} (µg/ml)
Fraction 1	> 100 (79.8%)[b]
Fraction 2	> 100 (94.9%)
Fraction 3	> 100 (74.3%)
Fraction 4	> 100 (66.1%)
Fraction 5	13.2 ± 1.7
Fraction 6	100 (55.0%)
Fraction 7	100 (53.3%)

Fraction 8	2.1 ± 0.8
Fraction 9	4.9 ± 3.8
Fraction 10	20.0 ± 4.1
Myricetin	2.7 ± 0.9[c]
EGCG	43.5 ± 4.2[c]
dsRNA 30 bp	0.012 ± 0.004[c]

[a]Extract/compound concentration required to inhibit rVP35 binding to dsRNA by 50%. Data show mean ± standard deviation of at least three independent experiments.
[b]Percentage of rVP35 control binding value to dsRNA in the presence of 100 µg/ml extract concentration.
[c]Concentration expressed in µM.

Given the complexity of the mixture, we could not exclude that some components of the whole natural extract or fractions could directly interact with the dsRNA, somehow contributing to the inhibition of the interaction between rVP35 and dsRNA. In order to better understand the mode-of-action, we moved forward on the identification of the main components of the active fractions. The active fractions were inspected by 1H NMR spectroscopy. The main component of Fraction 8 was the polyhydroxylated flavonoid myricetin (Figure 4.A), while the main component of Fraction 9 was (-)-epigallocatechin 3-O-gallate (EGCG) (Figure 4.B), and the fraction contained also a small percentage of myricetin. Both these fractions were further processed to isolate the pure compounds. Fraction 10 showed to contained mostly EGCG and traces of myricetin. Differently, Fraction 5 was actually a very complex mixture of compounds including esters of ferulic acid, caffeic acid, methyl gallate and several others components and it was obtained in considerably smaller amounts compared to the other fractions. Since Fraction 5 was 4-fold less potent than Fraction 8 and 9, it was not further investigated. We focused therefore our attention on the two main isolated components. Myricetin has been reported to have several biological effects since it i) inhibits the HIV-1 integrase (IN) [87], ii) inhibits HIV-1 reverse transcriptase (RT) [88], iii) has antioxidant and prooxidant activities that could increase damages of non-lipids components such carbohydrates and DNA, inducing DNA degradation, iv) possesses antiviral activities against viruses other than HIV-1 [89]. Differently, EGCG is the main catechin found in green tea, it is known to be a mitochondrion-targeting medicinal agent, regulating mitochondrial metabolism, including mitochondria-mediated cell cycle and apoptosis[90]. EGCG it has also been reported to possess antiviral properties on viruses from diverse families[91–95], and to reduce the DNA binding potency of nuclear antigen 1, hence impairing EBV infection[91].

These two molecules were tested by dose-response curves showing an IC_{50} value of 2.7 ± 0.9 and 43.5 ± 4.2 µM, respectively (table 2). Since it has been reported that flavonoids-like molecules, given their planar structure, can interact with dsDNA [96], it could be possible to speculate that these compounds can inhibit VP35-dsRNA binding by directly interacting with the dsRNA. However, on the one side myricetin has been shown to intercalate into dsDNA at concentrations greater than 300 µM, hence 100-fold higher than the observed IC_{50} value; on the other side, intercalation is considered more unlikely to happen in the case

of dsRNA. In fact, dsRNA has a weaker stretching rigidity versus the one of dsDNA, due to the stronger basepair inclination and slide in dsRNA [97]. Such hypothesis is also unlikely given the fact that other flavonoinds with intercalating properties similar to myricetin, such as luteolin, are inactive in our assay (data not shown), further confirming that the myricetin effect can't be linked to a hypothetic dsRNA binding.

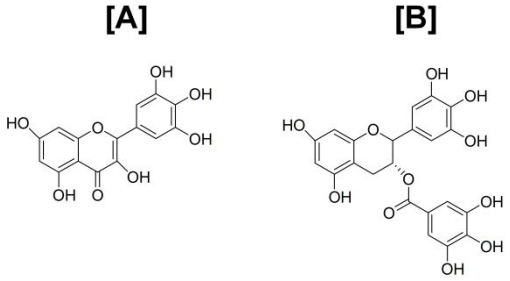

Figure. 4 [A] Myricetin chemical structure, [B] EGCG chemical structure.

Comparing the structures of the two compounds it is clear that the myricetin has an extensive network of conjugated sp^2 carbons that make the all structure almost planar, while the EGCG lacks of planarity on its chromane group and has a bulky gallate ester substituent that may negatively impact the binding.
In order to have some insights on the mode of action of the most promising ligand myricetin on the VP35-dsRNA interaction, a docking model of its binding within EBOV VP35 was then performed.

Myricetin inhibits EBOV VP35-dsRNA interaction by binding on RBD

Most docking algorithms are able to locate molecules according to experimental observations (X-Ray NMR), however their performance depends on the target [98]. It has been shown that consensus docking statistically improved the reliability of the docking results [99]. Therefore, we decided to use a consensus docking approach applying four molecular docking algorithms and analyzing the best poses of the active compound. In particular, we considered Glide [66], AutoDock [67], QMPL [68] and AutoDockVina [69] docking. The first important information obtained is that all programs placed the ligand in correspondence with the dsRNA binding site. Then we can suppose that myricetin acts directly inhibiting the viral dsDNA binding. This is not surprising since it has been shown in several studies that myricetin activity has a structural similarity with triphosphate substrates [100]. Another interesting aspect is that three out of four programs (all except AutodockVina) showed the same best binding pose (Figure. 5).

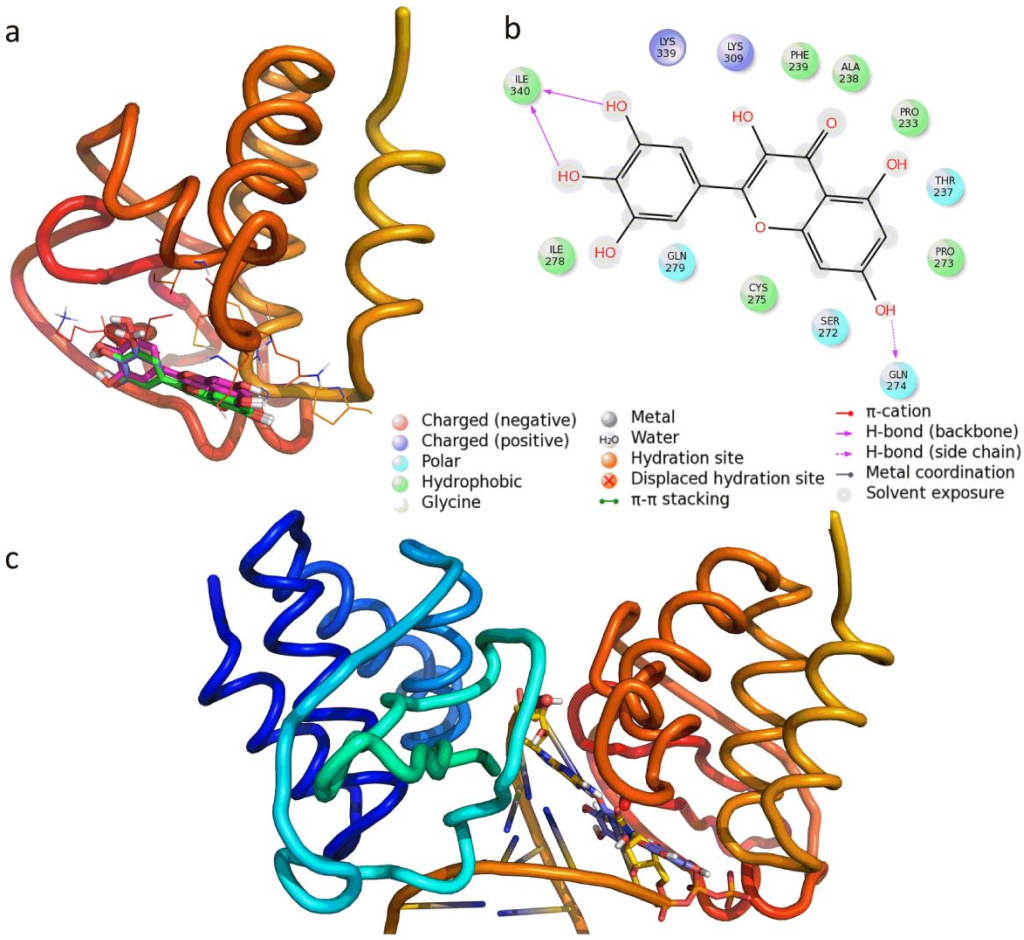

Figure. 5 Docking of Myricetin into the VP35 dsRNA binding pocket. [A] Putative binding mode of Myricetin in complex with VP35. The figure shows the Myricetin binding mode obtained with three docking programs (in green, magenta and violet); [B] 2D depictions of interactions of Myricetin with the VP35; [C] Superimposition of Myricetin complex (docking) with dsRNA-VP35 complex (pdb code 3l25): the ligand is shown in violet sticks while the terminal dsRNA bases are shown in yellow sticks.

For this reason, we can consider the predicted binding mode to be reliable and hence highlights the critical interactions that stabilize the myricetin-VP35 complex and to derive some considerations to design new and more active compounds. In particular, docking studies showed that myricetin could interact with important conserved residues in the RBD, establishing hydrogen bonds with Gln-274, with Ile-340, that is located in the β-sheet subdomain, and with Ala-238 and Ile-278 that are part of the α-helical subdomain (Fig. 5.B). In addition, the planar portions mimic the nucleoside while the OH mimics the sugar hydroxylic groups (Fig. 5.C). This information could help further optimization of this scaffold to improve the ligand affinity.

Finally, it is worth noting that most VP35 inhibitors reported so far act differently, binding to a pocket formed by residues from the α-helical and β-sheet subdomains including Ala221, Arg225, Gln241,

Leu242, Lys248, Lys251, Pro293, Ile295, Ile297, Asp302, and Phe328 which is reported to be important for NP interaction [28,101,102]. Considering that the VP35 pocket binding to dsRNA has also been involved with the interaction with other cellular factors such as PACT, IKK-ε and TBK-1 along the RIG-I pathway, as well as with other EBOV proteins such as NP, these results may suggest that small molecules interacting with this pocket could also be able to have multiple effects, impairing other VP35 functions in addition to its IFN antagonism.

CONCLUSIONS

In the present study, we established a new method for high-yield rVP35 expression and purification, and a new and robust fluorescence-based rVP35-RNA interaction assay (Z'-factor of 0.69) that will allow further biochemical characterization of the impact of VP35 structural changes on its dsRNA binding properties..Taking advantage to these methodologies, we identified the flavonoid compound myricetin, from the plant *L. morisianum*, as a powerful inhibitor of VP35 binding to dsRNA and showed that it binds to the VP35 dsRNA binding pocket with a new mechanism of action not yet explored that can offer the possibility of designing potent inhibitors. The development of myricetin derivatives with more potent anti-VP35 activity will be a good starting point to move further steps in the discovery of an effective anti-EVD therapeutic strategy.

ACKNOWLEDGEMENT

The authors would like to acknowledge Prof. Osvaldo Giorgi for useful discussions.

FUNDING

This work was supported by Sardinia Regional Government LR 07/2007 [CRP-78711/F72I15000900002] to [AC] and [AF] and [CRP2_682] to [LZ].

CONFLICT OF INTEREST

The authors declare no conflict of interest.

REFERENCES

(1) Baseler, L., Chertow, D. S., Johnson, K. M., Feldmann, H., and Morens, D. M. (2017) The Pathogenesis of Ebola Virus Disease. *Annu. Rev. Pathol. Mech. Dis. 12*, 387–418.

(2) Goldstein, T., Anthony, S. J., Gbakima, A., Bird, B. H., Bangura, J., Tremeau-Bravard, A., Belaganahalli, M. N., Wells, H. L., Dhanota, J. K., Liang, E., Grodus, M., Jangra, R. K., DeJesus, V. A., Lasso, G., Smith, B. R., Jambai, A., Kamara, B. O., Kamara, S., Bangura, W., Monagin, C., Shapira, S., Johnson, C. K., Saylors, K., Rubin, E. M., Chandran, K., Lipkin, W. I., and Mazet, J. A. K. (2018) The discovery of Bombali virus adds further support for bats as hosts of ebolaviruses. *Nat. Microbiol. 3*, 1084–1089.

(3) Kuhn, J. H., Becker, S., Ebihara, H., Geisbert, T. W., Johnson, K. M., Kawaoka, Y., Lipkin, W. I., Negredo, A. I., Netesov, S. V., Nichol, S. T., Palacios, G., Peters, C. J., Tenorio, A., Volchkov, V. E., and Jahrling, P. B. (2010) Proposal for a revised taxonomy of the family Filoviridae: Classification, names of taxa and viruses, and virus abbreviations. *Arch. Virol. 155*, 2083–2103.

(4) World Health Organization. (2016) EBOLA SITUATION REPORT.

(5) Centers for Disease Control and Prevention. (2016) Outbreaks Chronology: Ebola Virus Disease.

(6) Bray, M. (2003) Defense against filoviruses used as biological weapons. *Antiviral Res. 57*, 53–60.

(7) Reynolds, P., and Marzi, A. (2017) Ebola and Marburg virus vaccines. *Virus Genes*. 53, 501-515

(8) Wu, W., and Liu, S. (2017) The Drug Targets and Antiviral Molecules for Treatment of Ebola Virus Infection. *Curr. Top. Med. Chem. 17*, 361–370.

(9) Messaoudi, I., Amarasinghe, G. K., and Basler, C. F. (2015) Filovirus pathogenesis and immune evasion: Insights from Ebola virus and Marburg virus. *Nat. Rev. Microbiol.* 13, 663-76.

(10) Zinzula, L., and Tramontano, E. (2013) Strategies of highly pathogenic RNA viruses to block dsRNA detection by RIG-I-like receptors: Hide, mask, hit. *Antiviral Res.* 100, 615-635.

(11) Fanunza, E., Frau, A., Sgarbanti, M., Orsatti, R., Corona, A., and Tramontano, E. (2018) Development and validation of a novel dual luciferase reporter gene assay to quantify ebola virus VP24 inhibition of IFN signaling. *Viruses* 10, 98.

(12) Thompson, A. J. V, and Locarnini, S. a. (2007) Toll-like receptors, RIG-I-like RNA helicases and the antiviral innate immune response. *Immunol. Cell Biol. 85*, 435–45.

(13) Mühlberger, E., Weik, M., Volchkov, V. E., Klenk, H. D., and Becker, S. (1999) Comparison of the transcription and replication strategies of marburg virus and Ebola virus by using artificial replication systems. *J. Virol. 73*, 2333–42.

(14) Cannas, V., Daino, G. L. G. L., Corona, A., Esposito, F., and Tramontano, E. (2015) A Luciferase Reporter Gene Assay to Measure Ebola Virus Viral Protein 35–Associated Inhibition of Double-Stranded RNA–Stimulated, Retinoic Acid–Inducible Gene 1–Mediated Induction of Interferon β. *J. Infect. Dis. 212*, S277-281.

(15) Cardenas, W. B., Loo, Y.-M. Y.-M. Y.-M., Gale, M., Hartman, A. L., Kimberlin, C. R., Martinez-Sobrido, L., Saphire, E. O., Basler, C. F (2006) Ebola Virus VP35 Protein Binds Double-Stranded RNA and Inhibits Alpha/Beta Interferon Production Induced by RIG-I Signaling. *J. Virol. 80*, 5168–5178.

(16) Dilley, K. A., Voorhies, A. A., Luthra, P., Puri, V., Stockwell, T. B., Lorenzi, H., Basler, C. F., and Shabman, R. S. (2017) The Ebola virus VP35 protein binds viral immunostimulatory and host RNAs identified through deep sequencing. *PLoS One* (Lu, R., Ed.) *12*, e0178717.

(17) Luthra, P., Ramanan, P., Mire, C. E., Weisend, C., Tsuda, Y., Yen, B., Liu, G., Leung, D. W., Geisbert, T. W., Ebihara, H., Amarasinghe, G. K., and Basler, C. F. (2013) Mutual antagonism between the ebola virus VP35 protein and the RIG-I activator PACT determines infection outcome. *Cell Host Microbe*. 14, 74-84.

(18) Prins, K. C., Cárdenas, W. B., and Basler, C. F. (2009) Ebola virus protein VP35 impairs the function

of interferon regulatory factor-activating kinases IKKepsilon and TBK-1. *J. Virol. 83*, 3069–3077.
(19) Basler, C. F., Mikulasova, A., Martinez-Sobrido, L., Paragas, J., Mühlberger, E., Bray, M., Klenk, H.-D., Palese, P., and García-Sastre, A. (2003) The Ebola virus VP35 protein inhibits activation of interferon regulatory factor 3. *J. Virol. 77*, 7945–56.
(20) Bharaj, P., Atkins, C., Luthra, P., Giraldo, M. I., Dawes, B. E., Miorin, L., Johnson, J. R., Krogan, N. J., Basler, C. F., Freiberg, A. N., and Rajsbaum, R. (2017) The Host E3-Ubiquitin Ligase TRIM6 Ubiquitinates the Ebola Virus VP35 Protein and Promotes Virus Replication. *J. Virol.* (Lyles, D. S., Ed.) *91*, e00833-17.
(21) Le Sage, V., Cinti, A., McCarthy, S., Amorim, R., Rao, S., Daino, G. L., Tramontano, E., Branch, D. R., and Mouland, A. J. (2017) Ebola virus VP35 blocks stress granule assembly. *Virology*. 502, 73-83.
(22) Mitchell, W. M., and Carter, W. a. (2014) The quest for effective Ebola treatment: Ebola VP35 is an evidence-based target for dsRNA drugs. *Emerg. Microbes Infect. 3*, e77.
(23) Reid, S. P., Cárdenas, W. B., and Basler, C. F. (2005) Homo-oligomerization facilitates the interferon-antagonist activity of the ebolavirus VP35 protein. *Virology 341*, 179–89.
(24) Hartman, A. L., Towner, J. S., and Nichol, S. T. (2004) A C-terminal basic amino acid motif of Zaire ebolavirus VP35 is essential for type I interferon antagonism and displays high identity with the RNA-binding domain of another interferon antagonist, the NS1 protein of influenza a virus. *Virology*. 328, 177-184.
(25) Leung, D. W., Ginder, N. D., Fulton, D. B., Nix, J., Basler, C. F., Honzatko, R. B., and Amarasinghe, G. K. (2009) Structure of the Ebola VP35 interferon inhibitory domain. *Proc. Natl. Acad. Sci. U. S. A. 106*, 411–6.
(26) Leung, D. W., Shabman, R. S., Farahbakhsh, M., Prins, K. C., Borek, D. M., Wang, T., Mühlberger, E., Basler, C. F., and Amarasinghe, G. K. (2010) Structural and functional characterization of Reston Ebola virus VP35 interferon inhibitory domain. *J. Mol. Biol.* 399, 347-357.
(27) Kimberlin, C. R., Bornholdt, Z. A., Li, S., Woods, V. L., MacRae, I. J., and Saphire, E. O. (2010) Ebolavirus VP35 uses a bimodal strategy to bind dsRNA for innate immune suppression. *Proc. Natl. Acad. Sci. 107*, 314–319.
(28) Brown, C. S., Lee, M. S., Leung, D. W., Wang, T., Xu, W., Luthra, P., Anantpadma, M., Shabman, R. S., Melito, L. M., MacMillan, K. S., Borek, D. M., Otwinowski, Z., Ramanan, P., Stubbs, A. J., Peterson, D. S., Binning, J. M., Tonelli, M., Olson, M. A., Davey, R. A., Ready, J. M., Basler, C. F., and Amarasinghe, G. K. (2014) In silico derived small molecules bind the filovirus VP35 protein and inhibit its polymerase cofactor activity. *J. Mol. Biol. 426*, 2045–58.
(29) Basler, C. F., and Amarasinghe, G. K. (2009) Evasion of interferon responses by Ebola and Marburg viruses. *J. Interferon Cytokine Res. 29*, 511–520.
(30) Feng, Z., Cerveny, M., Yan, Z., and He, B. (2007) The VP35 Protein of Ebola Virus Inhibits the Antiviral Effect Mediated by Double-Stranded RNA-Dependent Protein Kinase PKR. *J. Virol. 81*, 182–92.
(31) Ramaswamy, V. K., Di Palma, F., Vargiu, A. V., Corona, A., Piano, D., Ruggerone, P., Zinzula, L.,

Tramontano, E. (2018) Insights into the homo-oligomerization properties of N-terminal coiled-coil domain of Ebola virus VP35 protein. *Virus Res. 247*, 61–70.

(32) Moller, P., Pariente, N., Klenk, H.-D., and Becker, S. (2005) Homo-Oligomerization of Marburgvirus VP35 Is Essential for Its Function in Replication and Transcription. *J. Virol. 79*, 14876–14886.

(33) Kirchdoerfer, R. N., Abelson, D. M., Li, S., Wood, M. R., and Saphire, E. O. (2015) Assembly of the Ebola Virus Nucleoprotein from a Chaperoned VP35 Complex. *Cell Rep. 12*, 140–149.

(34) Leung, D. W., Borek, D., Luthra, P., Binning, J. M., Anantpadma, M., Liu, G., Harvey, I. B., Su, Z., Endlich-Frazier, A., Pan, J., Shabman, R. S., Chiu, W., Davey, R. A., Otwinowski, Z., Basler, C. F., and Amarasinghe, G. K. (2015) An intrinsically disordered peptide from ebola virus VP35 controls viral RNA synthesis by modulating nucleoprotein-RNA interactions. *Cell Rep. 11*, 376–389.

(35) Zhu, T., Song, H., Peng, R., Shi, Y., Qi, J., and Gao, G. F. (2017) Crystal Structure of the Marburg Virus Nucleoprotein Core Domain Chaperoned by a VP35 Peptide Reveals a Conserved Drug Target for Filovirus. *J. Virol. 91*, e00996-17.

(36) Gire, Stephen K. , Goba A., A. K. G. et al. (2015) Genomic surveillance elucidates Ebola virus origin and transmission during the 2014 outbreak *345*, 1369–1372.

(37) Leung, D. W., Prins, K. C., Borek, D. M., Farahbakhsh, M., Tufariello, J. M., Ramanan, P., Nix, J. C., Helgeson, L. A., Otwinowski, Z., Honzatko, R. B., Basler, C. F., and Amarasinghe, G. K. (2010) Structural basis for dsRNA recognition and interferon antagonism by Ebola VP35. *Nat. Struct. Mol. Biol.* 17, 165-172

(38) Hartman, A. L., Bird, B. H., Towner, J. S., Antoniadou, Z.-A. Z.-A., Zaki, S. R., and Nichol, S. T. (2008) Inhibition of IRF-3 Activation by VP35 Is Critical for the High Level of Virulence of Ebola Virus. *J. Virol. 82*, 2699–2704.

(39) Prins, K. C., Delpeut, S., Leung, D. W., Reynard, O., Volchkova, V. A., Reid, S. P., Ramanan, P., Cardenas, W. B., Amarasinghe, G. K., Volchkov, V. E., and Basler, C. F. (2010) Mutations Abrogating VP35 Interaction with Double-Stranded RNA Render Ebola Virus Avirulent in Guinea Pigs. *J. Virol. 84*, 3004–3015.

(40) JACOBS, B. L., and Langland, J. O. (1996) When two strands are better than one: the mediators and modulators of the cellular responses to double-stranded RNA. *Virology 219*, 339–49.

(41) Zinzula, L., Esposito, F., Mühlberger, E., Trunschke, M., Conrad, D., Piano, D., and Tramontano, E. (2009) Purification and functional characterization of the full length recombinant Ebola virus VP35 protein expressed in E. coli. *Protein Expr. Purif.* 66, 113-119

(42) Zinzula, L., Esposito, F., Pala, D., and Tramontano, E. (2012) DsRNA binding characterization of full length recombinant wild type and mutants Zaire ebolavirus VP35. *Antiviral Res. 93, 354-363*

(43) Bale, S., Julien, J.-P. J.-P., Bornholdt, Z. A., Krois, A. S., Wilson, I. A., and Saphire, E. O. (2013) Ebolavirus VP35 Coats the Backbone of Double-Stranded RNA for Interferon Antagonism. *J. Virol. 87*, 10385–10388.

(44) Leung, D. W., Ginder, N. D., Nix, J. C., Basler, C. F., Honzatko, R. B., and Amarasinghe, G. K. (2009) Expression, purification, crystallization and preliminary X-ray studies of the Ebola VP35 interferon

inhibitory domain. *Acta Crystallogr. Sect. F Struct. Biol. Cryst. Commun. 65*, 163–165.
(45) Glanzer, J. G., Byrne, B. M., McCoy, A. M., James, B. J., Frank, J. D., and Oakley, G. G. (2016) In silico and in vitro methods to identify ebola virus VP35-dsRNA inhibitors. *Bioorg. Med. Chem.*
(46) Binning, J. M., Wang, T., Luthra, P., Shabman, R. S., Borek, D. M., Liu, G., Xu, W., Leung, D. W., Basler, C. F., and Amarasinghe, G. K. (2013) Development of RNA aptamers targeting Ebola virus VP35. *Biochemistry 52*, 8406–8419.
(47) Cragg, G. M., and Newman, D. J. (2013) Natural products: A continuing source of novel drug leads. *Biochim. Biophys. Acta - Gen. Subj. 1830*, 3670–3695.
(48) Atanasov, A. G., Waltenberger, B., Pferschy-Wenzig, E. M., Linder, T., Wawrosch, C., Uhrin, P., Temml, V., Wang, L., Schwaiger, S., Heiss, E. H., Rollinger, J. M., Schuster, D., Breuss, J. M., Bochkov, V., Mihovilovic, M. D., Kopp, B., Bauer, R., Dirsch, V. M., and Stuppner, H. (2015) Discovery and resupply of pharmacologically active plant-derived natural products: A review. *Biotechnol. Adv. 33*, 1582–1614.
(49) Arrigoni, P. V. (1983) Aspetti corologici della flora sarda. *Lav. della Soc. Ital. di Biogeogr. 8*, 83–109.
(50) Medail, F., and Quezel, P. (1999) Biodiversity Hotspots in the Mediterranean Basin: Setting Global Conservation Priorities. *Conserv. Biol. 13*, 1510–1513.
(51) Maxia, A., Sanna, C., Piras, A., Porcedda, S., Falconieri, D., Gonçalves, M. J., Cavaleiro, C., and Salgueiro, L. (2015) Chemical composition and biological activity of Tanacetum audibertii (Req.) DC. (Asteraceae), an endemic species of Sardinia Island, Italy. *Ind. Crops Prod. 65*, 472–476.
(52) Ornano, L., Venditti, A., Donno, Y., Sanna, C., Ballero, M., and Bianco, A. (2016) Phytochemical analysis of non-volatile fraction of *Artemisia caerulescens* subsp. *densiflora* (Viv.) (Asteraceae), an endemic species of La Maddalena Archipelago (Sardinia – Italy). *Nat. Prod. Res. 30*, 920–925.
(53) Venditti, A., Lattanzi, C., Ornano, L., Maggi, F., Sanna, C., Ballero, M., Alvino, A., Serafini, M., and Bianco, A. (2016) A new glucosidic phthalide from *Helichrysum microphyllum* subsp. *tyrrhenicum* from La Maddalena Island (Sardinia, Italy). *Nat. Prod. Res. 30*, 789–795.
(54) Formisano, C., Sanna, C., Ballero, M., Chianese, G., Sirignano, C., Rigano, D., Millán, E., Muñoz, E., and Taglialatela-Scafati, O. (2017) Anti-inflammatory sesquiterpene lactones from Onopordum illyricum L. (Asteraceae), an Italian medicinal plant. *Fitoterapia 116*, 61–65.
(55) Cagno, V., Sgorbini, B., Sanna, C., Cagliero, C., Ballero, M., Civra, A., Donalisio, M., Bicchi, C., Lembo, D., and Rubiolo, P. (2017) In vitro anti-herpes simplex virus-2 activity of Salvia desoleana Atzei & V. Picci essential oil. *PLoS One 12*, e0172322.
(56) Venditti, A., Sanna, C., Lorenzetti, L. M., Ballero, M., and Bianco, A. (2017) New Coumarinyl Ethers in Daphne oleoides Schreb. Collected from Sardinia Island. *Chem. Biodivers. 14*, e1700072.
(57) Mandrone, M., Scognamiglio, M., Fiorentino, A., Sanna, C., Cornioli, L., Antognoni, F., Bonvicini, F., and Poli, F. (2017) Phytochemical profile and α-glucosidase inhibitory activity of Sardinian Hypericum scruglii and Hypericum hircinum. *Fitoterapia 120*, 184–193.
(58) Esposito, F., Sanna, C., Del Vecchio, C., Cannas, V., Venditti, A., Corona, A., Bianco, A., Serrilli, A. M., Guarcini, L., Parolin, C., Ballero, M., and Tramontano, E. (2013) Hypericum hircinum L. components

as new single-molecule inhibitors of both HIV-1 reverse transcriptase-associated DNA polymerase and ribonuclease H activities. *Pathog. Dis. 68*, 116–24.
(59) Bylund, D. B., and Murrin, L. C. (2000) Radioligand saturation binding experiments over large concentration ranges. *Life Sci. 67*, 2897–2911.
(60) DeBlasi, A., O'Reilly, K., and Motulsky, H. J. (1989) Calculating receptor number from binding experiments using same compound as radioligand and competitor. *Trends Pharmacol. Sci. 10*, 227–229.
(61) Zhang, J.-H., Chung, and Oldenburg. (1999) A Simple Statistical Parameter for Use in Evaluation and Validation of High Throughput Screening Assays. *J. Biomol. Screen. 4*, 67–73.
(62) Mohamadi, F., Richards, N. G. J., Guida, W. C., Liskamp, R., Lipton, M., Caufield, C., Chang, G., Hendrickson, T., and Still, W. C. (1990) Macromodel-an integrated software system for modeling organic and bioorganic molecules using molecular mechanics. *J. Comput. Chem. 11*, 440–467.
(63) Halgren, T. A. (1996) Merck molecular force field. III. Molecular geometries and vibrational frequencies for MMFF94. *J. Comput. Chem. 17*, 553–586.
(64) Hasel, W., Hendrickson, T. F., and Still, W. C. (1988) A rapid approximation to the solvent accessible surface areas of atoms. *Tetrahedron Comput. Methodol. 1*, 103–116.
(65) Schrödinger LLC. (2018) Maestro GUI. New York (NY).
(66) Friesner, R. A., Murphy, R. B., Repasky, M. P., Frye, L. L., Greenwood, J. R., Halgren, T. A., Sanschagrin, P. C., and Mainz, D. T. (2006) Extra precision glide: Docking and scoring incorporating a model of hydrophobic enclosure for protein-ligand complexes. *J. Med. Chem. 49*, 6177–6196.
(67) Morris, G. M., Goodsell, D. S., Halliday, R. S., Huey, R., Hart, W. E., Belew, R. K., and Olson, A. J. (1998) Automated docking using a Lamarckian genetic algorithm and an empirical binding free energy function. *J. Comput. Chem. 19*, 1639–1662.
(68) Cho, A. E., Guallar, V., Berne, B. J., and Friesner, R. (2005) Importance of accurate charges in molecular docking: quantum mechanical/molecular mechanical (QM/MM) approach. *J. Comput. Chem. 26*, 915–31.
(69) Trott, O., and Olson, A. J. (2010) Software news and update AutoDock Vina: Improving the speed and accuracy of docking with a new scoring function, efficient optimization, and multithreading. *J. Comput. Chem. 31*, 455–461.
(70) Schrödinger LLC. (2014) The {PyMOL} Molecular Graphics System, Version 1.7.2.1.
(71) Swietnicki, W. (2006) Folding aggregated proteins into functionally active forms. *Curr. Opin. Biotechnol. 17*, 367–372.
(72) Grigorian, A. L., Bustamante, J. J., Hernandez, P., Martinez, A. O., and Haro, L. S. (2005) Extraordinarily stable disulfide-linked homodimer of human growth hormone. *Protein Sci. 14*, 902–913.
(73) Ramaswamy, V. K., Di Palma, F., Vargiu, A. V., Corona, A., Piano, D., Ruggerone, P., Zinzula, L., and Tramontano, E. (2018) Insights into the homo-oligomerization properties of N-terminal coiled-coil domain of Ebola virus VP35 protein. *Virus Res. 247*, 61–70.
(74) Leung, D. W., Prins, K. C., Basler, C. F., and Amarasinghe, G. K. (2010) Ebolavirus VP35 is a

multifunctional virulence factor. *Virulence*.1, 526-531.
(75) Yamamura, I. S. (1974) Muscarinic Cholinergic Binding in Rat Brain. *Proc. Natl. Acad. Sci. U. S. A. 71*, 1725–1729.
(76) Thermo Fisher Scientific Inc. (2011) Pierce ® Nickel Coated Plates Instructions.
(77) Motulsky, H. J., and Neubig, R. R. (2010) Analyzing binding data. in *Curr. Protoc. Neurosci.* pp 7.5.1-7.5.65 John Wiley & Sons, Inc., Hoboken
(78) Leung, D. W., Prins, K. C., Borek, D. M., Farahbakhsh, M., Tufariello, J. M., Ramanan, P., Nix, J. C., Helgeson, L. A., Otwinowski, Z., Honzatko, R. B., Basler, C. F., and Amarasinghe, G. K. (2010) Structural basis for dsRNA recognition and interferon antagonism by Ebola VP35. *Nat. Struct. Mol. Biol. 17*, 165–172.
(79) Derksen, A., Kühn, J., Hafezi, W., Sendker, J., Ehrhardt, C., Ludwig, S., and Hensel, A. (2016) Antiviral activity of hydroalcoholic extract from Eupatorium perfoliatum L. Against the attachment of influenza A virus. *J. Ethnopharmacol. 188*, 144–152.
(80) Xu, L., Grandi, N., Del Vecchio, C., Mandas, D., Corona, A., Piano, D., Esposito, F., Parolin, C., and Tramontano, E. (2015) From the traditional Chinese medicine plant Schisandra chinensis new scaffolds effective on HIV-1 reverse transcriptase resistant to non-nucleoside inhibitors. *J. Microbiol. 53*, 288–293.
(81) Wahyuni, T. S., Tumewu, L., Permanasari, A. A., Apriani, E., Adianti, M., Rahman, A., Widyawaruyanti, A., Lusida, M. I., Fuad, A., Fuchino, H., Kawahara, N., Shoji, I., Deng, L., Aoki, C., and Hotta, H. (2013) Antiviral activities of Indonesian medicinal plants in the East Java region against hepatitis C virus. *Virol. J. 10*, 1-9.
(82) Murray, A. P., Rodriguez, S., and Mulet, C. (2004) Antioxidant Metabolites from Limonium brasiliense (Boiss.) *Zeitschrift für Naturforschung C*, 59, 477–480.
(83) Aniya, Y., Miyagi, C., Nakandakari, A., Kamiya, S., Imaizumi, N., and Ichiba, T. (2002) Free radical scavenging action of the medicinal herb Limonium wrightii from the Okinawa islands. *Phytomedicine 9*, 239–244.
(84) Ksouri, R., Ksouri, W. M., Jallali, I., Debez, A., Magné, C., Hiroko, I., and Abdelly, C. (2011) Medicinal halophytes: potent source of health promoting biomolecules with medical, nutraceutical and food applications. *Crit. Rev. Biotechnol. 32*, 1–38.
(85) Medini, F., Ksouri, R., Falleh, H., Megdiche, W., and Trabelsi, N. (2011) Effects of physiological stage and solvent on polyphenol composition , antioxidant and antimicrobial activities of Limonium densiflorum *5*, 6719–6730.
(86) Sanna, C., Rigano, D., Corona, A., Piano, D., Formisano, C., Farci, D., Franzini, G., Ballero, M., Chianese, G., Tramontano, E., Taglialatela-Scafati, O., and Esposito, F. (2018) Dual HIV-1 reverse transcriptase and integrase inhibitors from Limonium morisianum Arrigoni, an endemic species of Sardinia (Italy). *Nat. Prod. Res.* 4, 1–6.
(87) Fesen, M. R., Pommier, Y., Leteurtre, F., Hiroguchi, S., Yung, J., and Kohn, K. W. (1994) Inhibition of HIV-1 integrase by flavones, caffeic acid phenethyl ester (CAPE) and related compounds. *Biochem.*

Pharmacol. 48, 595–608.
(88) Ono, K., Nakane, H., Fukushima, M., Chermann, J. C., and Barré-Sinoussi, F. (1990) Differential inhibitory effects of various flavonoids on the activities of reverse transcriptase and cellular DNA and RNA polymerases. *Eur. J. Biochem. 190*, 469–76.
(89) Ong, K. C., and Khoo, H.-E. (1997) Biological effects of myricetin. *Gen. Pharmacol. Vasc. Syst. 29*, 121–126.
(90) Shi, W., Li, L., Ding, Y., Yang, K., Chen, Z., Fan, X., Jiang, S., Guan, Y., Liu, Z., Xu, D., and Wu, L. (2018) The critical role of epigallocatechin gallate in regulating mitochondrial metabolism. *Future Med. Chem.* fmc-2017-0204.
(91) Chen, Y.-L., Tsai, H.-L., and Peng, C.-W. (2012) EGCG debilitates the persistence of EBV latency by reducing the DNA binding potency of nuclear antigen 1. *Biochem. Biophys. Res. Commun. 417*, 1093–1099.
(92) Yamaguchi, K., Honda, M., Ikigai, H., Hara, Y., and Shimamura, T. (2002) Inhibitory effects of (-)-epigallocatechin gallate on the life cycle of human immunodeficiency virus type 1 (HIV-1). *Antiviral Res. 53*, 19–34.
(93) Song, J.-M., Lee, K.-H., and Seong, B.-L. (2005) Antiviral effect of catechins in green tea on influenza virus. *Antiviral Res. 68*, 66–74.
(94) Colpitts, C. C., and Schang, L. M. (2014) A Small Molecule Inhibits Virion Attachment to Heparan Sulfate- or Sialic Acid-Containing Glycans. *J. Virol. 88*, 7806–7817.
(95) Pradhan, P., and Nguyen, M. L. (2018) Herpes simplex virus virucidal activity of MST-312 and epigallocatechin gallate. *Virus Res. 249*, 93–98.
(96) Snyder, R. D., and Gillies, P. J. (2002) Evaluation of the clastogenic, DNA intercalative, and topoisomerase II-interactive properties of bioflavonoids in Chinese hamster V79 cells. *Environ. Mol. Mutagen. 40*, 266–276.
(97) Bao, L., Zhang, X., Shi, Y.-Z., Wu, Y.-Y., and Tan, Z.-J. (2017) Understanding the Relative Flexibility of RNA and DNA Duplexes: Stretching and Twist-Stretch Coupling. *Biophys. J. 112*, 1094–1104.
(98) Wolf, A., Zimmermann, M., and Hofmann-Apitius, M. (2007) Alternative to Consensus ScoringA New Approach Toward the Qualitative Combination of Docking Algorithms. *J. Chem. Inf. Model. 47*, 1036–1044.
(99) Tuccinardi, T., Poli, G., Romboli, V., Giordano, A., and Martinelli, A. (2014) Extensive Consensus Docking Evaluation for Ligand Pose Prediction and Virtual Screening Studies. *J. Chem. Inf. Model. 54*, 2980–2986.
(100) Park, K.-S., Chong, Y., and Kim, M. K. (2016) Myricetin: biological activity related to human health. *Appl. Biol. Chem. 59*, 259–269.
(101) Ren, J.-X., Zhang, R.-T., Zhang, H., Cao, X.-S., Liu, L.-K., and Xie, Y. (2016) Identification of novel VP35 inhibitors: Virtual screening driven new scaffolds. *Biomed. Pharmacother. 84*, 199–207.
(102) Liu, G., Nash, P. J., Johnson, B., Pietzsch, C., Ilagan, M. X. G., Bukreyev, A., Basler, C. F., Bowlin,

T. L., Moir, D. T., Leung, D. W., and Amarasinghe, G. K. (2017) A Sensitive in Vitro High-Throughput Screen to Identify Pan-filoviral Replication Inhibitors Targeting the VP35-NP Interface. *ACS Infect. Dis. 3*, 190–198.

Identification of Myricetin as Ebolavirus VP35-dsRNA interaction inhibitor through a novel fluorescence-based assay

Gian Luca Daino[1], Aldo Frau[1], Cinzia Sanna[1], Daniela Rigano[2], Simona Distinto[1], Veronica Madau[1], Francesca Esposito[1], Elisa Fanunza[1], Giulia Bianco[1], Orazio Taglialatela-Scafati[2], Luca Zinzula[3], Elias Maccioni[1], Angela Corona[1] and Enzo Tramontano[1,4*]

For Table of Contents Use Only